Global patterns and climate drivers of terrestrial ecosystem water-use efficiency deduced from satellite products and carbon cycle models

Journal:	*Global Ecology and Biogeography*
Manuscript ID:	GEB-2014-0450
Manuscript Type:	Research Papers
Date Submitted by the Author:	14-Nov-2014
Complete List of Authors:	Sun, Yan; Peking University, Sino-French Institute for Earth System Science, College of Urban and Environmental Sciences Piao, Shilong; Peking University, Sino-French Institute for Earth System Science, College of Urban and Environmental Sciences; Chinese Academy of Sciences, Institute of Tibetan Plateau Research Huang, Mengtian; Peking University, Sino-French Institute for Earth System Science, College of Urban and Environmental Sciences Ciais, Philippe; CEA CNRS UVSQ, Laboratoire des Sciences du Climat et de l'Environnement Zeng, Zhenzhong; Peking University, Sino-French Institute for Earth System Science, College of Urban and Environmental Sciences Cheng, Lei; CSIRO, Land and Water Flagship Li, Xiran; Peking University, Sino-French Institute for Earth System Science, College of Urban and Environmental Sciences Zhang, Xinping; Peking University, Sino-French Institute for Earth System Science, College of Urban and Environmental Sciences Mao, Jiafu ; Oak Ridge National Laboratory, Climate Change Science Institute and Environmental Sciences Division Poulter, Ben; Montana State University, Institute on Ecosystems and the Department of Ecology Shi, Xiaoying; Oak Ridge National Laboratory, Climate Change Science Institute and Environmental Sciences Division Wang, Ying-Ping; CSIRO, Ocean and Atmosphere Flagship
Keywords:	Water-use Efficiency, inherent water-use efficiency, transpiration-based water-use efficiency, remote sensing, process-based model, climate drivers

Global patterns and climate drivers of terrestrial ecosystem water-use efficiency deduced from satellite products and carbon cycle models

Yan Sun[1], Shilong Piao[1,2*], Mengtian Huang[1], Philippe Ciais[3], Zhenzhong Zeng[1], Lei Cheng[4], Xiran Li[1], Xinping Zhang[1], Jiafu Mao[5], Ben Poulter[6], Xiaoying Shi[5], Ying-Ping Wang[7]

[1] Sino-French Institute for Earth System Science, College of Urban and Environmental Sciences, Peking University, Beijing 100871, China

[2] Institute of Tibetan Plateau Research, Chinese Academy of Sciences, Beijing 100085, China.

[3] LSCE, UMR CEA-CNRS, Bat. 709, CE, L'Orme des Merisiers, F-91191 Gif-sur-Yvette, France

[4] CSIRO Land and Water Flagship, GPO Box 1666, Canberra ACT 2601, 8 Australia

[4] Institute of Geographic Sciences and Natural Resources Research, Chinese Academy of Sciences, Beijing 100101, China

[5] Climate Change Science Institute and Environmental Sciences Division, Oak Ridge National Laboratory, Oak Ridge, TN 37831, USA

[6] Montana State University, Institute on Ecosystems and the Department of Ecology, Bozeman, Montana 59717, USA

[7] CSIRO Ocean and Atmosphere Flagship, PMB #1, Aspendale, Victoria 3195, Australia

Running title: Global patterns of Ecosystem WUE

Keywords: Water-use Efficiency, inherent water-use efficiency, transpiration-based water-use efficiency, remote sensing, process-based model, climate drivers

* Author for correspondence: Shilong Piao (slpiao@pku.edu.cn)

Abstract

Aim Ecosystem water-use efficiency (WUE), defined as the ratio of annual gross primary productivity (GPP) to annual evapotranspiration (ET), quantifies the water costs of ecosystem carbon acquisition through photosynthesis. Here, we investigated how ecosystem WUE varies spatially under different climate conditions, and how those variations of WUE differ from transpiration-based water-use efficiency (WUE_t) and transpiration-based inherent water-use efficiency ($IWUE_t$).

Location Global

Methods Two remote-sensing datasets of GPP and ET, and four process-based biosphere model estimates of GPP and ET.

Results Global WUE estimated by the two satellite datasets are 1.8 and 1.5 g C m^{-2} mm^{-1} respectively, which are lower than the simulations from four process-based models (2.0 ± 0.3 g C m^{-2} mm^{-1}). Model-estimated WUE is 16% and 22% higher than that derived from satellite data in tropical and temperate biomes, and even up to 53% higher in the boreal zone. Precipitation is the main control on the WUE spatial distribution for temperate and tropical regions, but temperature dominates in areas north of 50°N. The values of WUE, produced either from satellite datasets or model simulations, are higher in wetter regions with higher GPP. WUE_t exhibits a much lower, near-zero precipitation-sensitivity (S_P) than WUE. This finding is contrary to leaf and plant level observations of higher WUE_t in dry regions. Thus, we also calculated $IWUE_t$, the product of WUE_t and water vapour pressure deficit. $IWUE_t$ is found rather conservative with spatially increasing precipitation, in agreement with leaf and plant level measurements.

Main conclusions For arid ecosystems water losses are uncorrelated with vegetation productivity leading to lower WUE, whereas their control of canopy conductance is intrinsically efficient to maintain higher $IWUE_t$. Water-use efficiency as defined in three different ways produce different behavior, suggesting that separate responses of each water loss composition should be paid attention in comparing WUE trends.

INTRODUCTION

Photosynthesis is the largest component of the terrestrial carbon balance (Houghton, 2007). In this process CO_2 diffuses through leaf stomata and mesophyll cell walls and is assimilated into carbohydrate (Sage, 1994). At the same time as CO_2 is diffusing through leaf stomata, water vapour inside the leaf diffuses out as transpiration. Transpiration and photosynthesis are thus tightly coupled through leaf stomatal behaviour.

The coupling between carbon and water exchange at the leaf level can be quantified by ratio of its photosynthesis to transpiration, or water use efficiency at leaf scale. But at ecosystem scale, water-use efficiency (WUE) is generally defined as the ratio of annual gross primary production (GPP) to annual evapotranspiration (ET). ET includes: transpiration, water loss from canopy interception and bare soil evaporation. Ecosystem WUE is thus regulated by canopy conductance that is estimated by integrating leaf stomatal conductance over canopy leaf area index. Aerodynamic conductance and vegetation coverage also affect ecosystem WUE through determining the extent to which water and energy fluxes interact with the atmosphere (Jarvis & McNaughton, 1986). Water loss associated with ecosystem carbon assimilation can be divided into two components: (1) 'physiologically productive water' channeled through transpiration during the growing season; and (2) 'non-productive' water use: canopy interception and bare soil evaporation (Ponton *et al.*, 2006; Hu *et al.*, 2008). The partitioning of total ecosystem water loss between these productive and non-productive water uses can affect the coupling of water and carbon cycle at regional and global scales (Jackson *et al.*, 2005).

At leaf or canopy scale, optimal theories have been developed and used to explain quite successfully the responses of WUE to various environmental factors such as increased CO_2 and available soil water (Manzoni *et al.*, 2011; Medlyn *et al.*, 2011). Leaf WUE has been

observed or predicted to increase under mild water stress, which theoretically results from decreased stomatal conductance (Manzoni *et al*., 2011; Niu *et al.*, 2011). However, non-stomatal limitations, including reduced Rubisco activity and electron transport capacity, are also found to play a significant role in regulating leaf photosynthetic rate (Zhou *et al.,* 2013). As water stress becomes more severe, those internal controls will dominate, and reduce leaf WUE (Manzoni *et al*., 2011). Moreover, the response of leaf WUE to water stress varies among species owing to different water use strategies (Zhou *et al*., 2013).

At ecosystem scale, interactions between leaf physiology and canopy leaf area dynamics, carbon allocation and so on result in complex responses to changes in external environment (Niu *et al.,* 2008). Water loss by soil evaporation may respond to environmental change quite differently from transpiration at ecosystem scale. Furthermore, differences in ecological states related to stand age, plant type, structure and composition of ecosystems (Niu *et al.*, 2011) may lead to different water-use strategies by different ecosystems or under different climate conditions.

Although ecosystem-scale WUE has been measured and compared in many studies, no consistent conclusions have emerged about the variability of mean WUE across climate gradients. For example, some studies found that ecosystem WUE is higher in drier regions (Yu *et al.,* 2008; Lu & Zhuang, 2010; Ito & Inatomi, 2012), a finding which is consistent with that for leaf-scale responses, but contrary to the results based on eddy-covariance measurements of CO_2 and water fluxes by Hu *et al.* (2008), who found that ecosystem WUE increases increased with precipitation. By defining WUE as the ratio of aboveground net primary productivity (NPP) to ET, Ponce-Campos *et al.* (2013) found WUE a rather conservative mean quantity across different biomes. They also found that the response of ecosystem WUE to changes in precipitation varied over time, or WUE increased to a

maximum limit during drought, and decreased to a common value in wet years. Moreover, simulations by Tian *et al.* (2010) suggest that the relationship between WUE (calculated as the NPP to ET ratio) and annual mean precipitation is ecosystem-specific. For example, WUE decreased for wetland and cropland, but increased for forest and grassland ecosystems in response to an increase in precipitation.

Some of those diverging responses may be explained by the different definition of WUE. It brings difficulties to draw firm conclusions about the causes of spatial gradients in WUE at regional to global scale based on the results of previous studies. Furthermore responses of ecosystem WUE to environmental changes can vary in space and time (Ponce-Campos *et al.*, 2013). Contradictions between local studies can be partly due to their lack of spatial representativeness. In addition, many previous studies have empirically correlated WUE with precipitation gradients but ignored the confounding effects of temperature, radiation and nutrient availability (Hu *et al.,* 2008; Yu *et al.,* 2008; Ponce-Campos *et al.*, 2013). Therefore, those empirical relationships do allow us to gain further insight about the key controls of ecosystem WUE at different temporal and spatial scales.

In this study we investigated the global spatial patterns of ecosystem WUE. Spatial drivers and limiting climatic and ecological factors controlling WUE spatial variations were analyzed using a spatial regression analysis of WUE upon temperature, precipitation and solar radiation. Because temperature, rainfall and radiation co-vary spatially, multi-regression analysis between WUE and these three climate variables were used to identify the dominant global driver for regions under different climates. In addition, two other definitions (water uses transpiration-based water-use efficiency, i.e., WUE_t, and inherent water-use efficiency, i.e., $IWUE_t$) discriminating the productive water uses from non-productive water consumption

were used to investigate how different water uses affect the coupling of water and carbon cycles.

Material and methods

Data-driven GPP products

The MODIS and JUNG sets of gridded GPP data products are derived from climate and satellite data, and from satellite, climate and flux-tower data, respectively. MODIS GPP is estimated at 1 km spatial resolution from a light-use efficiency (LUE) model, as part of the operational MODIS algorithms (Running *et al.*, 2004) using meteorological data from NASA Data Assimilation Office and detailed vegetation information (land cover and FPAR) derived from the Moderate Resolution Imaging Spectroradiometer (MODIS) satellite from 2000 to present (Running *et al.*, 2004; Zhao *et al.*, 2005; Turner *et al.*, 2006). JUNG GPP is another data-oriented product derived by extrapolating the flux-tower observations from 178 sites in space and time using climate data and remotely sensed fAPAR data from 1982 to 2008 (Jung *et al.*, 2009). This latter monthly GPP product covers the period 1982-2008 at 0.5° spatial resolution, but many of the flux tower observations only cover much shorter periods.

Data-driven ET products

Global ET also cannot be measured directly at present, and are estimated using algorithms based on global meteorology data. MODIS ET is estimated using the Penman-Monteith approach with the enhanced vegetation index (EVI) fields from MODIS as input (Mu *et al.*, 2011; MOD16A2, http://www.ntsg.umt.edu/, accessed 16 September 2013). JUNG ET is another dataset based on model tree ensemble (MTE) regression, which extrapolates flux tower data as described for GPP above, yet with an additional correction for energy balance

closure assuming constant Bowen ratios (Jung *et al.*, 2010). The spatial resolution of MODIS ET and JUNG ET are same as their corresponding GPP products.

Process-based models

Process-based models incorporate empirical knowledge of mechanisms, and mass, water and energy conservation principles to simulate fluxes of CO_2 and water. Four models (CLM, CABLE, LPJ and ORCHIDEE) were used in this study at a global resolution of 0.5°. We use here the S2 simulation forced with the reconstructed climate fields CRU-NCEPv4 (http://dods.extra.cea.fr/data/p529viov/cruncep/) and annual CO_2 concentration over the period 1901-2012, but land use is kept constant at its present-day state. Different physiological processes controlling spatial gradients of WUE are incorporated in each model. Particularly, CLM and CABLE take into account the effect of nitrogen-limitation on ecosystem photosynthesis. Information about each model is presented in Table S1, and more details are given by Mao *et al.* (2013) for CLM, Wang *et al.* (2011) and Zhang *et al*. (2013) for CABLE, Sitch *et al.* (2003) for LPJ, and Krinner *et al.* (2005) for ORCHIDEE.

Analyses

GPP and ET from MODIS were re-gridded to 0.5° resolution using nearest-neighbour pixels. Monthly GPP and ET from remote-sensing data and from model simulations were summed to give annual totals. Mean annual GPP and ET were then calculated for the period from 2000 to the most recent year available (different time periods covered by each dataset, see Table S1). For both GPP and ET, the 0.5° grid cells with low productivity defined by a mean annual Normalized Difference Vegetation Index (NDVI, from AVHRR NDVI3g data) lower than 0.1 were discarded (11% of the land area).

Assuming homogeneous vegetation cover within each 0.5° grid cell, the ecosystem WUE was calculated as:

$$WUE = \frac{GPP}{ET} \quad (1)$$

with GPP in g C m^{-2} yr^{-1} and ET in mm yr^{-1}. For the remote-sensing datasets and process models, we used only GPP and ET produced or simulated consistently by each data-driven algorithm or model. Transpiration-based WUE (WUE_t) was defined as the ratio of annual GPP to annual transpiration (T) as:

$$WUE_t = \frac{GPP}{T} \quad (2)$$

T is only available from the process model outputs.

Previous studies by Beer et al. (2007, 2009) suggested that 'intrinsic water use efficiency', IWUE, that accounts for the effect of VPD on WUE should provide a better measure of ecosystem water use efficiency to other climatic variables:

$$IWUE = \frac{GPP \times VPD}{ET} \quad (3)$$

where VPD is the diurnal vapour pressure deficit (hPa) averaged over the growing season (defined here as the months when NDVI > 0.1) from Global Monitoring and Assimilation Office (GMAO, http://disc.sci.gsfc.nasa.gov/daac-bin/FTPSubset.pl). Mean inherent transpiration-based water use efficiency, $IWUE_t$, can then be calculated from the output of each model as:

$$IWUE_t = \frac{GPP \times VPD}{T} \quad (4)$$

Annual WUE in each 0.5° grid cell was projected in a two-dimensional space with mean annual temperature (MAT; ranging from -20 to 30°C as the horizontal axis) and mean annual

precipitation (MAP; ranging from 0 to 2000 mm as the vertical axis) binned into intervals of 0.5°C MAT and 20 mm MAP. For all grid cells within the same MAT and MAP pixel, area-weighted averages of GPP, ET and then WUE were calculated.

For the multiple regression analysis, spatial climate gradients were calculated using a moving window of 4.5°×4.5°, i.e., with the 81 pixels surrounding each 0.5° grid cell. The effects of precipitation, temperature, and radiation on WUE were estimated separately by controlling for the effects of other variables.

Results

Global WUE

Using two sets of satellite data products, we obtain an estimate of global WUE of 1.8 g C m^{-2} mm^{-1} and 1.5 g C m^{-2} mm^{-1}, from MODIS and JUNG data respectively (Fig. 1). Across different regions, estimates of WUE from MODIS are higher than those from JUNG in tropical (30°S-30°N) and temperate (30°N-50°N and 30°S-50°S) zones, but slightly lower in boreal area (50°N-90°N).

Process-based model simulations produce on average higher estimates (by ≈ 21%) of global WUE than those derived from remote sensing, particularly in boreal zone, where the mean estimate of WUE from process-based models is 54% higher than the estimate from the remote-sensing data products. The mean global WUE from different process-based models is estimated at 2.0 g C m^{-2} mm^{-1}, varying from 1.7 g C m^{-2} mm^{-1} by CLM to 2.3 g C m^{-2} mm^{-1} by LPJ.

Global spatial patterns of WUE

The two estimates of WUE derived from remote-sensing products both show large spatial variations (Figs 2a-b), with significant differences between different datasets, especially in dryland areas (MAP < 250 mm). WUE over northern Europe (ranging from 2.5 to 3.0 g C m^{-2} mm^{-1}), northern Eurasia (≈ 50°N), tropical rainforest areas and southeastern North America (temperate and sub-tropical) are consistently higher than other regions, while estimates of the WUE < 1.0 g C m^{-2} mm^{-1} are found in the Qinghai Tibet Plateau, India and northwestern North America.

Similar spatial patterns of WUE are simulated by the process-based models, although the estimates of WUE values from the results of four process-based models are much higher than estimates from remote-sensing products, especially in mid- and high latitude regions. For regions north of 50°N, the average WUE values over four model simulations are generally larger than 2.0 g C m^{-2} mm^{-1} and higher than data-driven ones by up to 40% (Figs 2g-h). However, WUE values over high latitudes vary greatly among different simulations, which ranging from < 0.5 g C m^{-2} mm^{-1} for CLM to > 3.5 g C m^{-2} mm^{-1} for LPJ (Figs 2c-f).

Variation of the sensitivities of WUE to MAP and MAT

Spatial variations of WUE with MAT and MAP are quite similar between the estimates from satellite data and process-based models (see Fig. 3). Globally, estimates of WUE using both methods are highest in regions with optimal hydro-thermal conditions (i.e., the certain ratios of MAP to MAT). However, estimate of WUE from remote-sensing products is maximal at a MAP of ≈ 1300 mm and MAT between 5 to 10°C (Fig. 3a), while maximal WUE estimates from the process-based models are found in regions with MAP in the range of 600-800 mm and MAT between 2 and 6°C (Fig. 3b).

However, variations of WUE with MAP or MAT, measured by precipitation-sensitivity (S_P) and temperature-sensitivity (S_T), from two different approaches are quite different (insets of Fig. 3). S_P is positive for the results from both remote-sensing products and process-based models, even in the cold regions with MAT lower than 0°C. But, S_P estimated from remote-sensing products decreases with MAT when MAT < 10°C, then increases with MAT when 10°C < MAT < 15°C, and decreases with MAT when MAT > 15°C (Fig. 3a). In contrast, S_P estimated from process-based models increases with MAT when -10°C < MAT <10°C, then remains almost constant when MAT > 10°C (Fig. 3b). In terms of S_T, remote-sensing products present positive values in arid regions with MAP less than 200 mm but show significantly negative values in wet regions where MAP > 1000 mm (Fig. 3a), while the process models always exhibit negative values across the entire MAP range (Fig. 3b).

Geographical spatial sensitivity of WUE to climate variables

In climate space, multiple regression analysis shows that WUE is significantly ($p < 0.05$) positively related to precipitation for ≈ 40% of the vegetated land both in the remote-sensing products and in the models (Fig. 4a, 4b). Positive correlation mainly occurs south of 50°N, with lower S_P (< 1‰ mm^{-1}; $p < 0.05$) found in humid areas and higher values (> 4‰ mm^{-1}; $p < 0.05$) in drier regions such as the western United States, central Asia and dry areas of northeast Asia. At high latitudes (60°N - 90°N), WUE over ≈ 40% of the pixels ($p < 0.05$) is negatively associated with increasing precipitation. The biggest differences in the WUE-MAP spatial correlation between remote-sensing data and models are found for tropical drylands. In these regions, model-simulated WUE is significantly positive correlated with MAP, while remote-sensing estimated WUE responds negatively to MAP (Fig. S2). Moreover, for tropical rainforests, modelled WUE is positively correlated with precipitation; but estimates from the

remote-sensing products show spatially varying responses to changing precipitation, with much weaker sensitivity than that from model simulations.

Both remote-sensing and model results show broadly consistent variation of WUE with MAT (Figs 4c-d). Generally, WUE is positively correlated with temperature at high latitudes (about 50% pixels north of 50°N ; $p < 0.05$), with S_T ranging from 5% °C^{-1} to 20% °C^{-1} from remote-sensing products, but smaller S_T of less than 10% °C^{-1} from model results. On the contrary, WUE is negatively correlated with MAT over ≈ 30% ($p < 0.05$) of the pixels south of 50°N. For tropical rainforest ecosystems, the remote-sensing products and model results consistently produce a weak negative sensitivity of WUE to temperature (S_T > -10% °C^{-1}; $p < 0.05$).

In terms of the impact of mean annual solar downward radiation (R_S), both remote-sensing and model WUE results show positive correlations between WUE and R_S over 20% to 30% ($p < 0.05$) pixels north of 50°N, with radiation-sensitivity (S_R) higher than 6% per W m^{-2} (Figs 4e-f). However, negative correlations dominate in the low and mid-latitude regions with considerable variation of S_R ranging from near-zero to values < -6% per W m^{-2}. S_R in mid-latitudes (-1% per W m^{-2} ~ -3% per W m^{-2}) is larger in magnitude than in tropical forest regions (> -1% per W m^{-2}). In addition, data-driven results show positive S_R over most of Australia, part of North Africa and southern North America, which contradict with model simulations.

DISCUSSION

Major differences between data-driven and modelled WUE

The two WUE estimations based on remote-sensing datasets differ from each other in both global mean values and spatial patterns, especially for regions with low ET, such as tropical

drylands. Differences of WUE between MODIS and JUNG are primarily attributable to their systematic differences in estimated ET. ET produced by MODIS is considerably lower in dry areas but generally higher in humid regions than JUNG ET. These differences in ET lead to great differences in the magnitude of WUE, as well as spatial gradients of WUE between MODIS- and JUNG-based estimates. Uncertainties in ET estimated from remote-sensing can have a number of causes such as: ignoring terrestrial water storage terms, the lack of energy balance closure in flux-tower datasets, and landscape-level heterogeneity (Zeng *et al.*, 2012). In addition, biases in GPP from satellite products also lead to errors in WUE estimates. MODIS and JUNG all use satellite fAPAR to drive empirical models for GPP, but this methodology is considered to be uncertain because cloudiness can cause unspecified biases in fAPAR (Baret *et al.*, 2007). Moreover, Lee *et al.* (2013) found that enhanced vegetation index (EVI) in Amazon remains high, whereas sun-induced chlorophyll fluorescence (SIF) from GOSAT SIF suggests a decrease in GPP during the dry season. Thus GPP estimates made using current fAPAR can be positively biased in tropical regions. For GPP derived from JUNG, uncertainty increases for boreal and tropical regions, where few flux sites are located.

Compared with remote-sensing based WUE, model estimates are generally higher (Fig. 1, Fig. 2), indicating that some of the processes involved are poor simulations of the actual physiological and ecological mechanisms. As shown by Fig. 5, averaged GPP across four models is 28% higher than remote-sensing derived GPP, whereas mean modelled ET is not significantly different from the data-driven result. Moreover, differences in modelled processes such as carbon-nitrogen interactions, soil depth maps, root profiles, and soil water holding capacity parameters, as well as different function of water stress (Sulman *et al.,* 2012) are all responsible for the different coupling between GPP and ET in each model, and thus lead to larger uncertainties in WUE estimates.

Nutrient resource availability also regulates plant productivity (Cleveland *et al.,* 2013) as well as other ecosystem processes, and eventually impacts WUE. Fisher *et al*. (2012) even inverted regions with nutrient limitation from NDVI deviations from a maximum NDVI-ET slope, which is close to a maximum envelope for WUE. Previous studies on the temporal change of productivity concluded that nitrogen limitation reduces the response of GPP to elevated atmospheric CO_2 (Thornton *et al*., 2007; Zaehle *et al.*, 2014). Spatially, the insufficient availability of nitrogen is widespread in terrestrial vegetation (Wang *et al.*, 2010) and nitrogen limitation increases from the tropics to high latitudes (Wang *et al.*, 2010). Wang *et al.* (2010) estimated that net primary productivity (NPP) is reduced by 35% - 40% at high latitudes by nitrogen limitation and reported that simulations without considering the nitrogen limitation overestimate NPP by about 29%. For tropical ecosystems, the impact of nitrogen limitation on plant growth is weaker, because in tropical ecosystems ~ 18% of NPP is contributed by external nitrogen inputs (Cleveland *et al.,* 2013). Some studies have also suggested that phosphorus rather than nitrogen limitation constrains NPP across much of the tropics where nitrogen is plentiful (Wang *et al.*, 2010; Cleveland *et al.,* 2013); this is because new phosphorus inputs are very small relative to plant demand in the tropics (Cleveland *et al.,* 2013).

Failure to include human disturbance in the models may also leads to biases in vegetation productivity. None of the models used for this study take land-use change into account; the models may thus contain much too great an area of forest and hence higher simulated GPP (Bondeau et al., 2007). Neglecting air pollution also causes a reduction in modelled GPP by deteriorating physiological and ecological processes. Although many studies have reported that nitrogen limitation significantly suppresses ET through reducing leaf area and stomatal conductance under photosynthesis down-regulation (Lee *et al.*, 2013), our comparison

between remote-sensing based and modelled ET shows no evident high-bias in the model simulations (Fig. 5b).

Spatial pattern of WUE

With the exception of the patterns estimated from MODIS, the spatial distributions of WUE estimated from different datasets consistently show higher values in wetter environments (Fig. 2). For mid- and low latitude ecosystems with seasonal water-limitation (Huxman *et al.*, 2004), WUE spatial gradients are controlled by precipitation rather than by temperature and radiation (Fig. S2). The positive sensitivity of WUE to precipitation gradually declines from desert, through mesic, to humid regions as soil water stress decreases. Semi-arid and mesic areas, limited by soil water availibility, can utilize higher precipitation to sustain GPP more efficiently than wetter regions (Huxman *et al.*, 2004). The enhancement of ET is less than that of GPP per unit of precipitation increase, which results in a higher WUE for wetter areas when going from arid to mesic climates. For humid regions such as northern Europe and tropical rainforest, where ecosystems have a high WUE, any increase in precipitation in excess of plant demand becomes runoff, which may even deplete nutrients available for plant growth through leaching (Huxman *et al.*, 2004; Posada & Schuur, 2011). More cloudiness during precipitation also decreases R_S, which consequently limits GPP (Scanlon & Albertson, 2004). In the context of long-term adaptation in areas with abundant precipitation, plants with higher resources use efficiency, especially for nutrients rather than water, have a competitive advantage in long-term selection (Huxman *et al.*, 2004). Ecological studies of NPP also point out that nitrogen mineralization, water uptake by plants and productivity (NPP) are optimally adjusted to each other (Roy *et al.*, 2001). As a result, WUE tends to be controlled by the strongest limiting factor. The existence of other limiting factors for WUE results in spatially inconsistent responses of the sensitivity of WUE to precipitation between models and

remote-sensing results (Figs S2a-b). Without considering nutrient limitation, models predict that WUE is enhanced as precipitation increases; therefore WUE can be positively correlated with precipitation even for rainforest (Figs 4a-b). GPP of ecosystems at high latitudes often is co-limited by temperature and radiation instead of precipitation (Figs 4c-f). For those cold regions, air temperature and incoming solar radiation limit GPP, they are positively correlated with ecosystem productivity (Piao *et al.*, 2007) and hence lead to higher WUE. However, observations of the carbon cycle from GOSAT (Frankenberg *et al.,*2011) suggested that MODIS and JUNG underestimate GPP in the tropics for savannas where no flux tower observations are available at present, and overestimate GPP in arctic regions. So it is possible that estimates of GPP from MODIS and JUNG are too high in tropical forest and boreal forest, and too low in savannas. This would change the spatial pattern of WUE.

Most current models and observations indicate that transpiration dominates the terrestrial water flux emitted to the atmosphere (Lawrence, 2007; Jasechko *et al.,* 2013). Based on this, previous studies used ET, expecting it to be close to T, to calculate ecosystem WUE. However, few observation sites are located in arid regions with annual precipitation less than 200 mm, at such sites bare soil evaporation contributes most to ET, and acts to decrease WUE. Our results (Fig. 3) show that mean WUE increases with precipitation along climate gradients, which contradicts evidence from WUE observations at leaf and plant scale that water stress is found to reduce T per unit of GPP.

To explore whether the inclusion of bare soil evaporation in ET results in this discrepancy, we used model simulations to calculate the transpiration-based water use efficiency (WUE_t) given by equation (2). WUE_t in climate space still shows higher values with larger precipitation (Fig. 6a), except for cold regions with MAT < 0°C, indicating that the lower WUE in dry regions is not only determined by the increased soil evaporation. This finding is

consistent with canopy-scale studies (Baldocchi, 1994; Hu *et al.*, 2008), which pointed out that WUE_t at canopy scale is mainly controlled by photosynthetic capacity (i.e., GPP) instead of T. The denser canopies of vegetation growing in humid conditions have both larger light-bearing surfaces and higher light use efficiency (Hu *et al.,* 2008). Thus vegetation will benefit from the increased diffuse radiation (Knohl & Baldocchi, 2008), and hence increase GPP per unit of water loss. However, we also found that, in climate space, modelled values of S_P for WUE_t are generally positive but very close to zero, except for cold regions with MAT < 0°C, indicating that arid ecosystems take a number of strategies to reduce transpiration to maintain normal physiological activities during dry seasons (Monasterio & Sarmiento, 1976).

Increased water vapour pressure deficit at the leaf surface has been found to reduce leaf WUE (Linderson *et al.*, 2012). Similar responses have also been observed at canopy or ecosystem scale (Ponton *et al.*, 2006; Niu *et al.*, 2011; Linderson *et al.*, 2012). In order to remove the effects of both bare soil evaporation and VPD, here, we now use transpiration-based inherent water-use efficiency ($IWUE_t$, equation 4) to investigate variations of modelled $IWUE_t$ with MAP and MAT. A quite different modelled $IWUE_t$-MAP spatial relationship is observed to that found for WUE and shows that $IWUE_t$ displays negative, but very close to zero, S_P for warm regions with MAT > 10°C (Fig. 6b). This finding basically agrees with the leaf WUE conclusion of higher WUE_t being found in dry regions, where drought-tolerant species with physiological advantages in resisting drought and holding water dominate the ecosystem (Zhou *et al*., 2013). For arid regions, more water vapour flux is allocated to bare soil evaporation (Hu *et al*., 2008) and intensive transpiration driven by high VPD. This high water cost, uncorrelated with vegetation productivity, leads to relatively lower WUE in dry areas than in wetter areas, though modelled plants in these regions conserve a higher $IWUE_t$ than in mesic and humid climates. In contrast, for wet regions with high vegetation coverage and high air humidity, most of the water consumption is closely bound up with vegetation productivity

and hence leads to a higher WUE. Moreover, long-term natural selection, i.e., ecosystem adaptation to local climate and nutrient status (Huxman *et al.*, 2004), shaped the optimal vegetation composition (Still *et al.*, 2003) and essentially determined the spatial pattern of WUE.

Considering that poor representation of eco-physiological mechanisms in the models may lead to unrealistic conclusions, we calculated satellite product IWUE (equation 3) to test the validity of the model results. A lower S_P was also estimated by data-driven IWUE than WUE, despite negative values found with MAT > 20°C owing to an extremely low MODIS-ET product (Fig. S2a). These results suggest that the 'intrinsic changes' of water and carbon correlation actually exist in ecosystems. IWUE derived from models (Fig. S2b) shows a generally similar climatic pattern, except for dry areas with MAP < 200 mm but higher S_P across the whole MAT range with the satellite result. This response to precipitation is different from that estimated from modelling $IWUE_t$ (Fig. 6b) with negative but near-zero S_P across the whole MAT range, indicating the important influence of evaporation on WUE behaviour. Consistent IWUE-MAP relationships derived from satellite products and models demonstrates that the conclusions from our calculation of water-use efficiency based on transpiration (WUE_t, $IWUE_t$) are broadly credible in explaining the spatial patterns of WUE.

ACKNOWLEDGEMENT

This study was supported by the National Natural Science Foundation of China (41125004), National Basic Research Program of China (2013CB956303), Chinese Ministry of Environmental Protection Grant (201209031), the 111 Project (B14001), and National Youth Top-notch Talent Support Program in China. Jiafu Mao and Xiaoying Shi's time is supported by the US Department of Energy (DOE), Office of Science, Biological and Environmental Research. Oak Ridge National Laboratory is managed by UT-BATTELLE for DOE under

contract DE-AC05-00OR22725. The simulation of CLM is supported by the US Department of Energy (DOE), Office of Science, Biological and Environmental Research. Oak Ridge National Laboratory is managed by UT-BATTELLE for DOE under contract DE-AC05-00OR22725.

References

Baldocchi, D. (1994) A comparative study of mass and energy exchange rates over a closed C_3 (wheat) and an open C_4(corn) crop: II. CO_2 exchange and water use efficiency. *Agricultural and Forest Meteorology*, **67**, 291-321.

Baret, F., Hagolle, O., Geiger, B., Bicheron, P., Miras, B., Huc, M., Berthelot, B., Niño, F., Weiss, M., Samain, O., Roujean, J.L. & Leroy, M. (2007) LAI, fAPAR and fCover CYCLOPES global products derived from VEGETATION: Part 1: Principles of the algorithm. *Remote Sensing of Environment*, **110**, 275-286.

Beer, C., Ciais, P., Reichstein, M., Baldocchi, D., Law, B.E., Papale, D., Soussana, J.F., Ammann, C., Buchmann, N., Frank, D., Gianelle, D., Janssens, I.A., Knohl, A., Köstner, B., Moors, E., Roupsard, O., Verbeeck, H., Vesala, T., Williams, C.A. & Wohlfahrt, G. (2009) Temporal and among-site variability of inherent water use efficiency at the ecosystem level. *Global Biogeochemical Cycles*, **23**, GB2018, doi: 10.1029/2008GB003233.

Beer, C., Reichstein, M., Ciais, P., Farquhar, G.D. & Papale, D. (2007) Mean annual GPP of Europe derived from its water balance. *Geophysical Research Letters*, **34**, L05401, doi: 10.1029/2006GL029006.

Berry, J.A., Beerling, D.J. & Franks, P.J. (2010) Stomata: key players in the earth system, past and present. *Current opinion in plant biology*, **13**, 232-239.

Bondeau, A., Smith, P.C., Zaehle, S., Schaphoff, S., Lucht, W., Cramer, W., Gerten, D., Lotze-Campen, H., MÜLler, C., Reichstein, M. & Smith, B. (2007) Modelling the role of agriculture for the 20th century global terrestrial carbon balance. *Global Change Biology*, **13**, 679-706.

Cleveland, C.C., Houlton, B.Z., Smith, W.K., Marklein, A.R., Reed, S.C., Parton, W., Del Grosso, S.J. & Running, S.W. (2013) Patterns of new versus recycled primary

production in the terrestrial biosphere. *Proceedings of the National Academy of Sciences of the United States of America*, **110**, 12733-12737.

Fisher, J.B., Badgley, G. & Blyth, E. (2012) Global nutrient limitation in terrestrial vegetation. *Global Biogeochemical Cycles*, **26**, GB3007, doi: 10.1029/2011GB004252.

Frankenberg, C., Fisher, J.B., Worden, J., Badgley, G., Saatchi, S.S., Lee, J.-E., Toon, G.C., Butz, A., Jung, M., Kuze, A. & Yokota, T. (2011) New global observations of the terrestrial carbon cycle from GOSAT: Patterns of plant fluorescence with gross primary productivity. *Geophysical Research Letters*, **38**, L17706, doi: 10.1029/2011GL048738.

Houghton, R.A. (2007) Balancing the Global Carbon Budget. *Annual Review of Earth and Planetary Sciences*, **35**, 313-347.

Hu, Z., Yu, G., Fu, Y., Sun, X., Li, Y., Shi, P., Wang, Y. & Zheng, Z. (2008) Effects of vegetation control on ecosystem water use efficiency within and among four grassland ecosystems in China. *Global Change Biology*, **14**, 1609-1619.

Huxman, T.E., Smith, M.D., Fay, P.A., Knapp, A.K., Shaw, M.R., Loik, M.E., Smith, S.D., Tissue, D.T., Zak, J.C. & Weltzin, J.F. (2004) Convergence across biomes to a common rain-use efficiency. *Nature*, **429**, 651-654.

Ito, A. & Inatomi, M. (2012) Water-use efficiency of the terrestrial biosphere: a model analysis focusing on interactions between the global carbon and water cycles. *Journal of Hydrometeorology*, **13**, 681-694.

Jackson, R.B., Jobbágy, E.G., Avissar, R., Roy, S.B., Barrett, D.J., Cook, C.W., Farley, K.A., Le Maitre, D.C., McCarl, B.A. & Murray, B.C. (2005) Trading water for carbon with biological carbon sequestration. *Science*, **310**, 1944-1947.

Jarvis, P.G. & McNaughton, K. (1986) Stomatal control of transpiration: scaling up from leaf to region. *Advances in ecological research*, **15**, 1-49.

Jasechko, S., Sharp, Z.D., Gibson, J.J., Birks, S.J., Yi, Y. & Fawcett, P.J. (2013) Terrestrial water fluxes dominated by transpiration. *Nature*, **496**, 347-350.

Jung, M., Reichstein, M. & Bondeau, A. (2009) Towards global empirical upscaling of FLUXNET eddy covariance observations: validation of a model tree ensemble approach using a biosphere model. *Biogeosciences*, **6**, 2001-2013.

Jung, M., Reichstein, M., Ciais, P., Seneviratne, S.I., Sheffield, J., Goulden, M.L., Bonan, G., Cescatti, A., Chen, J., de Jeu, R., Dolman, A.J., Eugster, W., Gerten, D., Gianelle, D., Gobron, N., Heinke, J., Kimball, J., Law, B.E., Montagnani, L., Mu, Q., Mueller, B., Oleson, K., Papale, D., Richardson, A.D., Roupsard, O., Running, S., Tomelleri, E., Viovy, N., Weber, U., Williams, C., Wood, E., Zaehle, S. & Zhang, K. (2010) Recent decline in the global land evapotranspiration trend due to limited moisture supply. *Nature*, **467**, 951-954.

Knohl, A. & Baldocchi, D.D. (2008) Effects of diffuse radiation on canopy gas exchange processes in a forest ecosystem. *Journal of Geophysical Researchn G: Biogeosciences*, **113**, G02023, doi: 10.1029/2007JG000663.

Krinner, G., Viovy, N., de Noblet-Ducoudré, N., Ogée, J., Polcher, J., Friedlingstein, P., Ciais, P., Sitch, S. & Prentice, I.C. (2005) A dynamic global vegetation model for studies of the coupled atmosphere-biosphere system. *Global Biogeochemical Cycles*, **19**, GB1015, doi: 10.1029/2003GB002199.

Lawrence, D.M., Thornton, P.E., Oleson, K.W. & Bonan, G.B. (2007) The partitioning of evapotranspiration into transpiration, soil evaporation, and canopy evaporation in a GCM: Impacts on land-atmosphere interaction. *Journal of Hydrometeorology*, **8**, 862-880.

Lee, E., Felzer, B.S. & Kothavala, Z. (2013) Effects of nitrogen limitation on hydrological processes in CLM4-CN. *Journal of Advances in Modeling Earth Systems*, **5**, 741-754.

Lee, J.-E., Frankenberg, C., van der Tol, C., Berry, J.A., Guanter, L., Boyce, C.K., Fisher, J.B., Morrow, E., Worden, J.R. & Asefi, S. (2013) Forest productivity and water stress in Amazonia: observations from GOSAT chlorophyll fluorescence. *Proceedings of the Royal Society B: Biological Sciences*, **280**, 20130171.

Linderson, M.-L., Mikkelsen, T.N., Ibrom, A., Lindroth, A., Ro-Poulsen, H. & Pilegaard, K. (2012) Up-scaling of water use efficiency from leaf to canopy as based on leaf gas exchange relationships and the modeled in-canopy light distribution. *Agricultural and Forest Meteorology*, **152**, 201-211.

Lu, X. & Zhuang, Q. (2010) Evaluating evapotranspiration and water-use efficiency of terrestrial ecosystems in the conterminous United States using MODIS and AmeriFlux data. *Remote Sensing of Environment*, **114**, 1924-1939.

Manzoni, S., Vico, G., Katul, G., Fay, P.A., Polley, W., Palmroth, S. & Porporato, A. (2011) Optimizing stomatal conductance for maximum carbon gain under water stress: a meta-analysis across plant functional types and climates. *Functional Ecology*, **25**, 456-467.

Mao, J., Shi, X., Thornton, P.E., Hoffman, F.M., Zhu, Z. & Myneni, R.B. (2013) Global latitudinal-asymmetric vegetation growth trends and their driving mechanisms: 1982–2009. *Remote Sensing*, **5**, 1484-1497.

Medlyn, B.E., Duursma, R.A., Eamus, D., Ellsworth, D.S., Prentice, I.C., Barton, C.V., Crous, K.Y., de Angelis, P., Freeman, M. & Wingate, L. (2011) Reconciling the optimal and empirical approaches to modelling stomatal conductance. *Global Change Biology*, **17**, 2134-2144.

Monasterio, M. & Sarmiento, G. (1976) Phenological strategies of plant species in the tropical savanna and the semi-deciduous forest of the Venezuelan Llanos. *Journal of Biogeography*, 325-355.

Mu, Q., Zhao, M. & Running, S.W. (2011) Improvements to a MODIS global terrestrial evapotranspiration algorithm. *Remote Sensing of Environment*, **115**, 1781-1800.

Niu, S., Wu, M., Han, Y., Xia, J., Li, L. & Wan, S. (2008) Water-mediated responses of ecosystem carbon fluxes to climatic change in a temperate steppe. *New Phytologist*, **177**, 209-219.

Niu, S., Xing, X., Zhang, Z., Xia, J., Zhou, X., Song, B., Li, L. & Wan, S. (2011) Water-use efficiency in response to climate change: from leaf to ecosystem in a temperate steppe. *Global Change Biology*, **17**, 1073-1082.

Piao, S., Friedlingstein, P., Ciais, P., Viovy, N. & Demarty, J. (2007) Growing season extension and its impact on terrestrial carbon cycle in the Northern Hemisphere over the past 2 decades. *Global Biogeochemical Cycles*, **21**, GB3018, doi: 10.1029/2006GB002888.

Ponce-Campos, G.E., Moran, M.S., Huete, A., Zhang, Y., Bresloff, C., Huxman, T.E., Eamus, D., Bosch, D.D., Buda, A.R. & Gunter, S.A. (2013) Ecosystem resilience despite large-scale altered hydroclimatic conditions. *Nature*, **494**, 349-352.

Ponton, S., Flanagan, L.B., Alstad, K.P., Johnson, B.G., Morgenstern, K., Kljun, N., Black, T.A. & Barr, A.G. (2006) Comparison of ecosystem water-use efficiency among Douglas-fir forest, aspen forest and grassland using eddy covariance and carbon isotope techniques. *Global Change Biology*, **12**, 294-310.

Posada, J.M. & Schuur, E.A. (2011) Relationships among precipitation regime, nutrient availability, and carbon turnover in tropical rain forests. *Oecologia*, **165**, 783-795.

Roy, J., Mooney, H.A. & Saugier, B. (2001) *Terrestrial Global Productivity*. Academic Press.

Running, S.W., Nemani, R.R., Heinsch, F.A., Zhao, M.S., Reeves, M. & Hashimoto, H. (2004) A continuous satellite-derived measure of global terrestrial primary production. *Bioscience*, **54**, 547-560.

Sage, R.F. (1994) Acclimation of photosynthesis to increasing atmospheric CO2: the gas exchange perspective. *Photosynthesis research*, **39**, 351-368.

Scanlon, T.M. & Albertson, J.D. (2004) Canopy scale measurements of CO2 and water vapor exchange along a precipitation gradient in southern Africa. *Global Change Biology*, **10**, 329-341.

Shi, X., Mao, J., Thornton, P.E. & Huang, M. (2013) Spatiotemporal patterns of evapotranspiration in response to multiple environmental factors simulated by the Community Land Model. *Environmental Research Letters*, **8**, 024012.

Sitch, S., Smith, B., Prentice, I.C., Arneth, A., Bondeau, A., Cramer, W., Kaplan, J., Levis, S., Lucht, W. & Sykes, M.T. (2003) Evaluation of ecosystem dynamics, plant geography and terrestrial carbon cycling in the LPJ dynamic global vegetation model. *Global Change Biology*, **9**, 161-185.

Still, C.J., Berry, J.A., Collatz, G.J. & DeFries, R.S. (2003) Global distribution of C3 and C4 vegetation: carbon cycle implications. *Global Biogeochemical Cycles*, **17**, 6-1-6-14.

Sulman, B.N., Desai, A.R., Schroeder, N.M., Ricciuto, D., Barr, A., Richardson, A.D., Flanagan, L.B., Lafleur, P.M., Tian, H., Chen, G., Grant, R.F., Poulter, B., Verbeeck, H., Ciais, P., Ringeval, B., Baker, I.T., Schaefer, K., Luo, Y. & Weng, E. (2012) Impact of hydrological variations on modeling of peatland CO2 fluxes: Results from the North American Carbon Program site synthesis. *Journal of Geophysical Research: Biogeosciences*, **117**, G01031, doi: 10.1029/2011JG001862.

Thornton, P.E., Lamarque, J.-F., Rosenbloom, N.A. & Mahowald, N.M. (2007) Influence of carbon-nitrogen cycle coupling on land model response to CO2 fertilization and

climate variability. *Global Biogeochemical Cycles*, **21**, GB4018, doi: 10.1029/2006GB002868.

Tian, H., Chen, G., Liu, M., Zhang, C., Sun, G., Lu, C., Xu, X., Ren, W., Pan, S. & Chappelka, A. (2010) Model estimates of net primary productivity, evapotranspiration, and water use efficiency in the terrestrial ecosystems of the southern United States during 1895–2007. *Forest Ecology and Management*, **259**, 1311-1327.

Turner, D.P., Ritts, W.D., Cohen, W.B., Gower, S.T., Running, S.W., Zhao, M.S., Costa, M.H., Kirschbaum, A.A., Ham, J.M., Saleska, S.R. & Ahl, D.E. (2006) Evaluation of MODIS NPP and GPP products across multiple biomes. *Remote Sensing of Environment*, **102**, 282-292.

Wang, Y., Kowalczyk, E., Leuning, R., Abramowitz, G., Raupach, M.R., Pak, B., van Gorsel, E. & Luhar, A. (2011) Diagnosing errors in a land surface model (CABLE) in the time and frequency domains. *Journal of Geophysical Research G: Biogeosciences*, **116**, G01034, doi: 10.1029/2010JG001385.

Wang, Y., Law, R. & Pak, B. (2010) A global model of carbon, nitrogen and phosphorus cycles for the terrestrial biosphere. *Biogeosciences*, **7**, 2261-2282.

Yu, G., Song, X., Wang, Q., Liu, Y., Guan, D., Yan, J., Sun, X., Zhang, L. & Wen, X. (2008) Water-use efficiency of forest ecosystems in eastern China and its relations to climatic variables. *New Phytologist*, **177**, 927-937.

Zaehle, S., Medlyn, B.E., De Kauwe, M.G., Walker, A.P., Dietze, M.C., Hickler, T., Luo, Y., Wang, Y.P., El‐Masri, B. & Thornton, P. (2014) Evaluation of 11 terrestrial carbon-nitrogen cycle models against observations from two temperate Free-Air CO_2 Enrichment studies. *New Phytologist*, **202**, 803-822.

Zeng, Z., Piao, S., Lin, X., Yin, G., Peng, S., Ciais, P. & Myneni, R.B. (2012) Global evapotranspiration over the past three decades: estimation based on the water balance equation combined with empirical models. *Environmental Research Letters*, **7**, 014026.

Zhang, Q., Pitman, A., Wang, Y., Dai, Y. & Lawrence, P. (2013) The impact of nitrogen and phosphorous limitation on the estimated terrestrial carbon balance and warming of land use change over the last 156 yr. *Earth System Dynamics*, **4**, 333-345.

Zhao, M., Heinsch, F.A., Nemani, R.R. & Running, S.W. (2005) Improvements of the MODIS terrestrial gross and net primary production global data set. *Remote sensing of Environment*, **95**, 164-176.

Zhou, S., Duursma, R.A., Medlyn, B.E., Kelly, J.W. & Prentice, I.C. (2013) How should we model plant responses to drought? An analysis of stomatal and non-stomatal responses to water stress. *Agricultural and Forest Meteorology*, **182**, 204-214.

BIOSKECH

Yan Sun is a PhD candidate at Peking University, Beijing, China. She has broad research interests particularly in vegetation dynamics and the carbon balance of terrestrial ecosystems. She also maintains interests in nitrogen and phosphorus cycles.

Figure legends

Figure 1 Total water-use efficiency (WUE) estimations for global, boreal (50°N-90°N), tropical (30°S-30°N) area and temperate zone of the Northern Hemisphere (30°N-50°N) and Southern Hemisphere (30°S-50°S) from two sets of observed evapotranspiration (ET) and gross primary productivity (GPP) products and four global models. Error bars indicate interannual standard deviations.

Figure 2 Global spatial patterns of land WUE derived from: (a, b) coupled remote-sensing dataset and (c-f) process-based models, averaged from 2000 to the most recent year available (see Table S1). (g) Mean WUE values estimated by data-driven products and (h) simulated mean WUE across four models are also shown. Values of mean annual Normalized Difference Vegetation Index (NDVI) below 0.1 are screened out.

Figure 3 Distribution of mean WUE in mean annual temperature (MAT) – mean annual precipitation (MAP) domain: (a) remote-sensing data, (b) process-based models. The bottom insets show the MAP-sensitivity across the MAT range. Black lines in insets refer to the absolute changes of WUE (slope calculated from simple linear regression between WUE and MAP under same MAT interval) along the MAP gradient. Red lines represent the relative changes (calculated as absolute slope value divided by mean WUE of all MAP-zones with same small range of MAT) of WUE. Grey scale indicates uncertainties among two data-driven results and four models results, in which the darkest zones represent largest uncertainty. Similarly, the left insets show the MAT-sensitivity across the MAP range.

Figure 4 Spatial sensitivity of WUE to: (a, b) precipitation, (c, d) temperature and (e, f) solar radiation, based on remote-sensing data (a, c, e) and process models (b, d, f). Only statistically significant ($p < 0.05$) correlations are shown.

Figure 5 Comparisons between products from data-driven and outputs simulated by process models: (a) mean GPP and (b) mean ET, the colour bar shows the point intensity.

Figure 6 Distribution of (a) mean transpiration-based water-use efficiency (WUE_t) and (b) transpiration-based inherent water-use efficiency ($IWUE_t$) in MAT-MAP domain from process-based models. The bottom insets show the MAP-sensitivity (red lines) across the MAT range and the grey scale indicates uncertainties among four model results, in which the darkest zones represent largest uncertainty. Similarly, the left insets show the MAT-sensitivity across the MAP range.

Figure 1

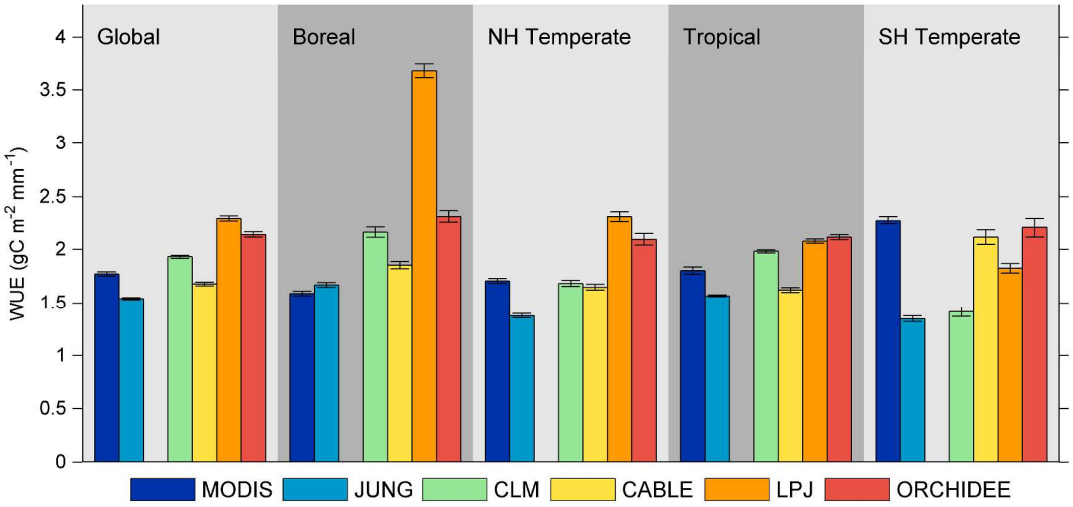

650 **Figure 2**

651

652

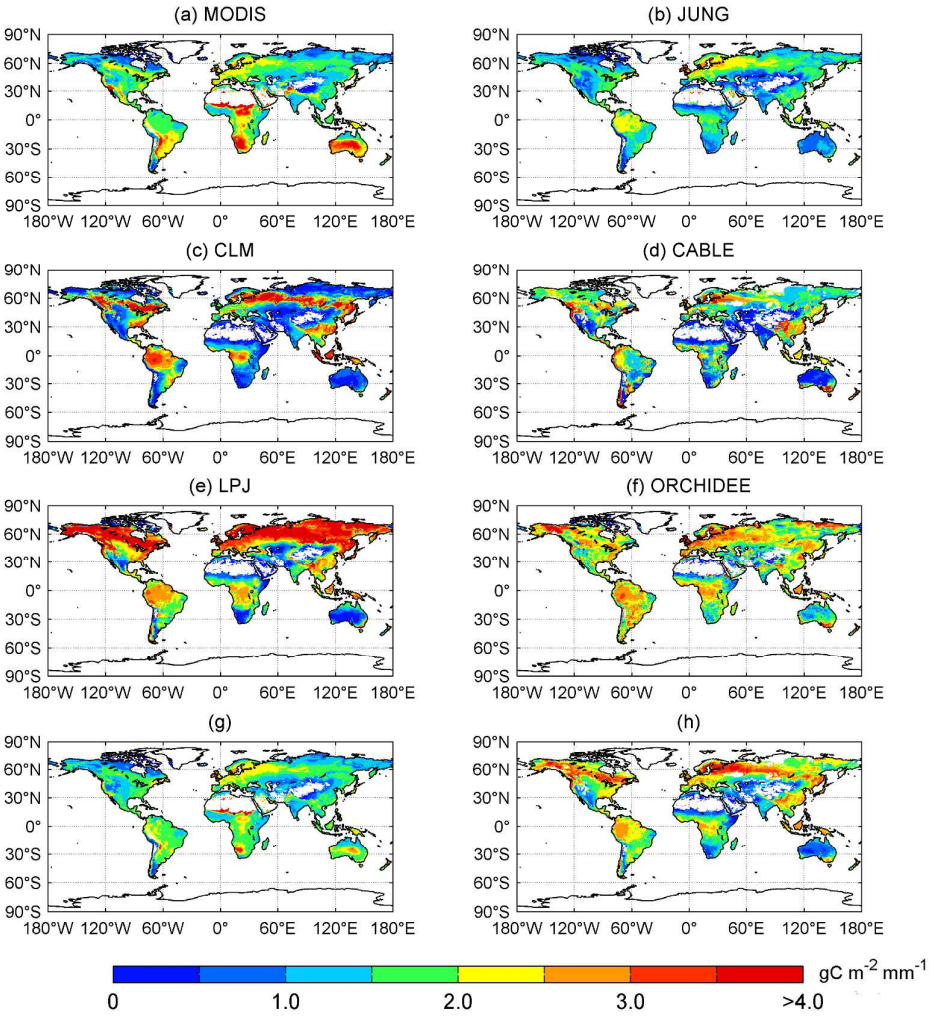

653 **Figure 3**

654

655

656

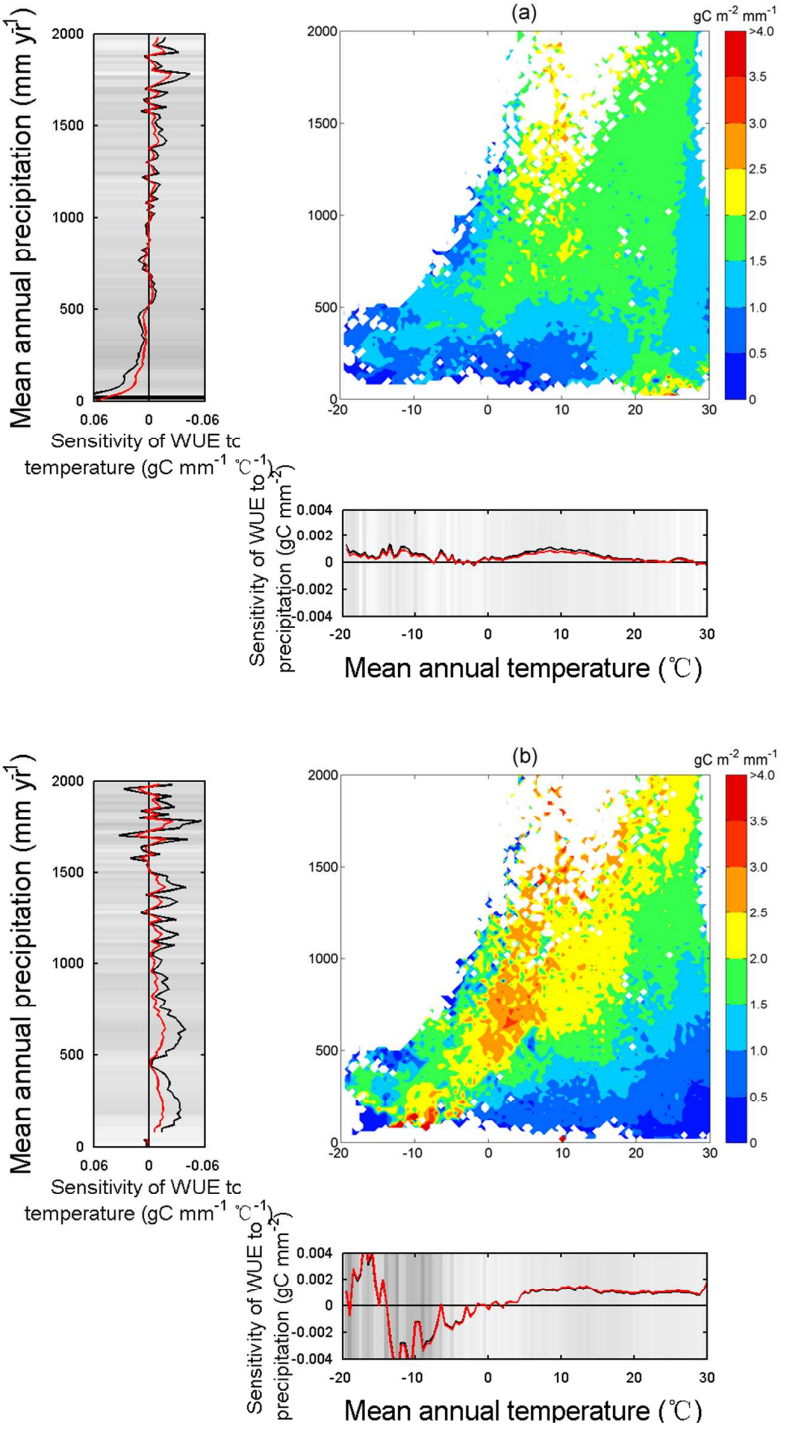

Figure 4

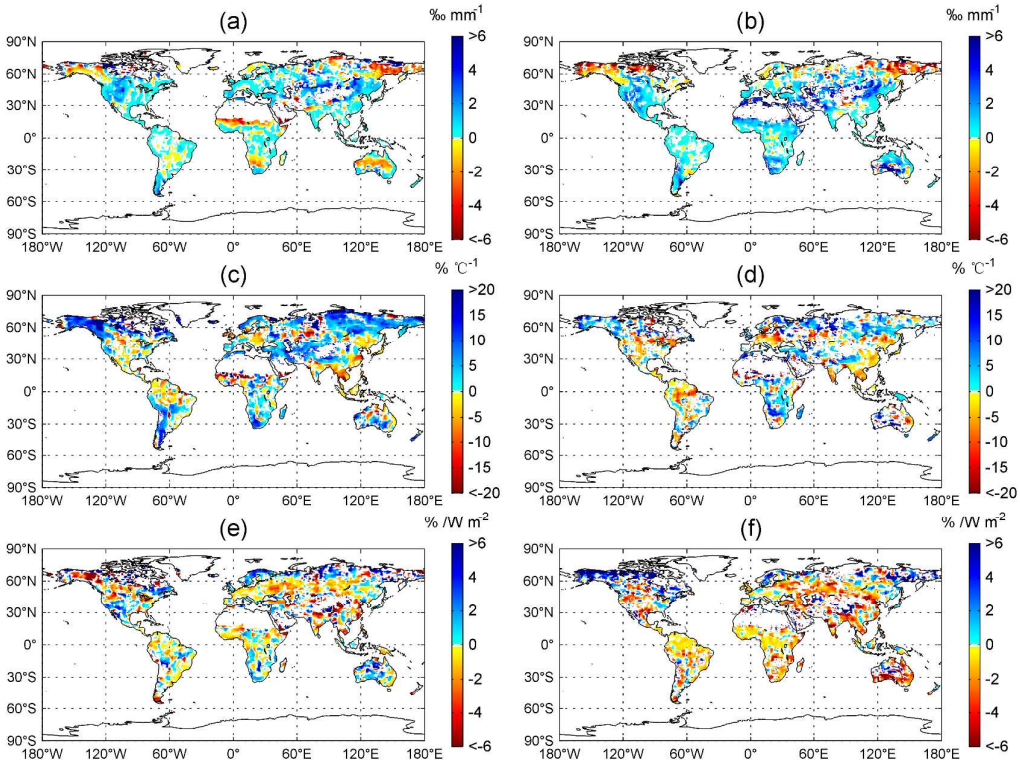

660 **Figure 5**

661

662

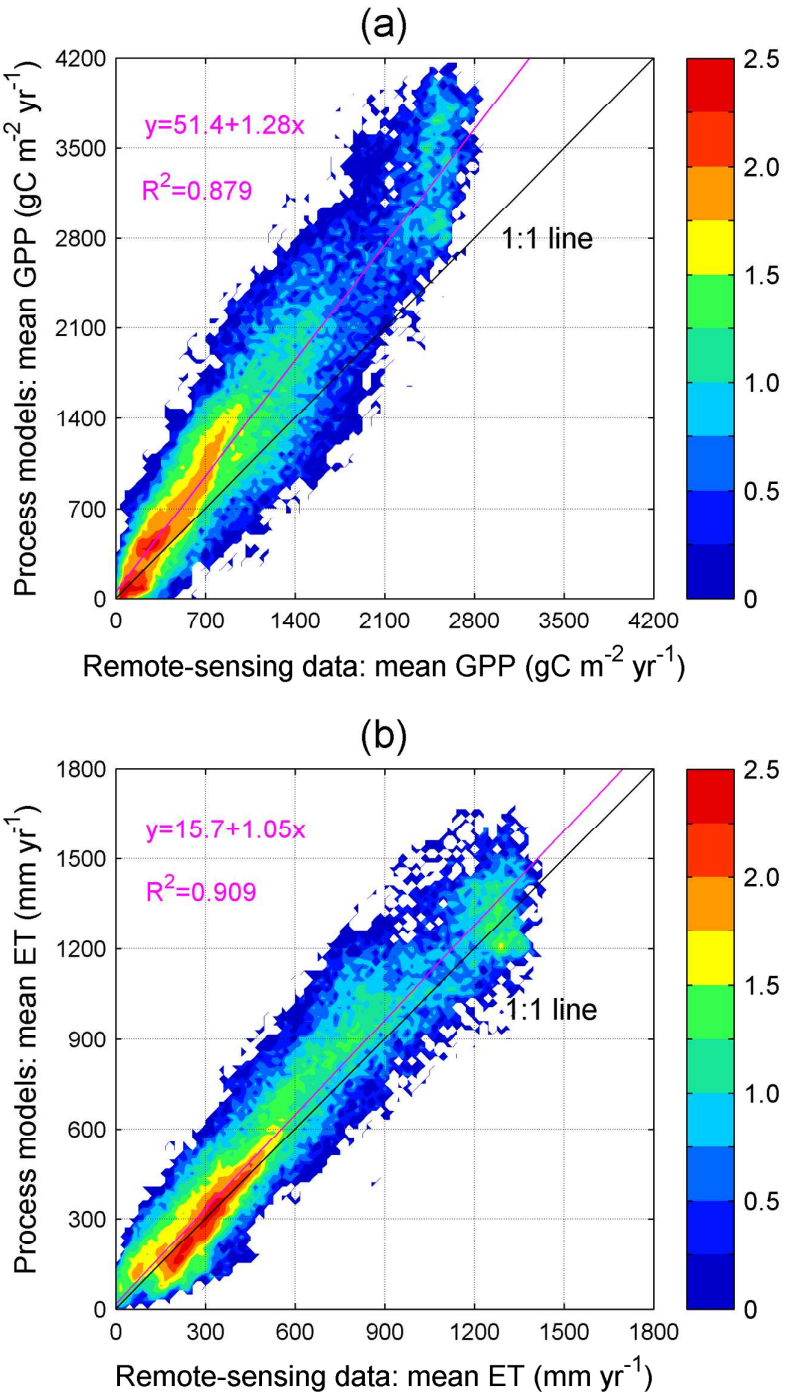

663 **Figure 6**

664